Selection shapes the genomic landscape of introgressed ancestry in a pair of sympatric sea urchin species

Matthew R. Glasenapp[*1], Grant H. Pogson[1]
[1]Department of Ecology and Evolutionary Biology, University of California, Santa Cruz

[*]Corresponding author: mglasena at ucsc dot edu

Abstract

A growing number of recent studies have demonstrated that introgression is common across the tree of life. However, we still have a limited understanding of the fate and fitness consequence of introgressed variation at the whole-genome scale across diverse taxonomic groups. Here, we implemented a phylogenetic hidden Markov model to identify and characterize introgressed genomic regions in a pair of well-diverged, non-sister sea urchin species: *Strongylocentrotus pallidus* and *S. droebachiensis*. Despite the old age of introgression, a sizable fraction of the genome (1% - 5%) exhibited introgressed ancestry, including numerous genes showing signals of historical positive selection that may represent cases of adaptive introgression. There were two chromosomes with considerably reduced introgression and a negative correlation between introgression and gene density, consistent with selection against introgression. Testing for nonrandom patterns among introgressed regions relative to the non-introgressed genome-wide background revealed that introgressed regions had significantly reduced nucleotide divergence (d_{XY}) and overlapped fewer protein-coding genes, coding bases, and genes with a history of positive selection. Additionally, genes residing within introgressed regions showed slower rates of evolution (d_N, d_S, d_N/d_S) than random distributions of genes without introgressed ancestry. Overall, our findings are consistent with widespread selection against introgressed ancestry across the genome and suggest that slowly evolving, low-divergence genomic regions are more likely to move between species and avoid negative selection following hybridization and introgression.

Introduction

Advances in genome sequencing have revealed that many species hybridize with close relatives and share alleles through introgression. However, relatively little is known about the fate and fitness consequence of introgressed variation at the whole-genome scale. Although it has been well established that introgression often facilitates adaptation (Song et al. 2011; The Heliconius Genome Consortium 2012; Huerta-Sánchez et al. 2014; Lamichhaney et al. 2015; Arnold et al. 2016), studies documenting adaptive introgression often focus on phenotypes that were known *a priori* to have been involved in adaptation (Martin and Jiggins 2017). Despite enthusiasm about the potential for introgression to introduce new alleles already tested by selection at a frequency higher than mutation (Hedrick 2013; Martin and Jiggins 2017), there remain few estimates of the proportion of introgressed ancestry fixed by positive selection across entire genomes.

A promising approach to understanding the overall fitness consequence of introgression involves identifying and characterizing genomic regions showing introgressed ancestry. Genome-wide scans for introgression have demonstrated that the distribution of introgressed haplotypes across the genome, termed the genomic landscape of introgression, is highly heterogeneous due to the combined effects of natural selection and recombination. Most introgressed variation is thought to be deleterious and removed by selection because it either (i) is maladapted to the recipient's ecology (i.e., ecological selection; McBride and Singer 2010; Arnegard et al. 2014; Cooper et al. 2018), (ii) causes negative epistasis in the genomic background of the recipient (i.e., hybrid incompatibilities; Orr 1995), or (iii) imposes a genetic load on the recipient if the donor has a smaller effective population size (i.e., hybridization load; Harris and Nielsen 2016; Juric et al. 2016; but see Kim et al. 2018). Selection against

introgression should lead to a positive correlation between introgression and recombination because recombination weakens the strength of selection acting on introgressed variation by breaking up long introgression tracts with multiple linked, deleterious alleles and distributing introgressed ancestry more evenly among individuals (Barton 1983; Harris and Nielsen 2016; Veller et al. 2023). Numerous empirical studies have demonstrated a positive correlation between introgression and the local recombination rate (Brandvain et al. 2014; Schumer et al. 2016; Ravinet et al. 2018; Martin et al. 2019; Calfee et al. 2021; Ravinet et al. 2021). However, few organismal groups have been studied, and some notable exceptions exist, including a negative correlation between local recombination rate and admixed ancestry in *Drosophila melanogaster* (Pool 2015; Corbett-Detig and Nielsen 2017).

Gene density is also thought to influence the distribution of introgressed ancestry, as the strength of selection depends on the density of selected sites (Barton 1983; Barton and Bengtsson 1986; Martin and Jiggins 2017). Reduced rates of introgression near functionally important elements have been found in diverse groups, such as humans (Sankararaman et al. 2014; Juric et al. 2016; Sankararaman et al. 2016; Petr et al. 2019), house mice (Teeter et al. 2008; Janoušek et al. 2015), *Histoplasma* fungi (Maxwell et al. 2018), wild strawberries (Feng et al. 2023), and *Xiphophorus* swordtails (Schumer et al. 2016). It is important to note that gene density and recombination rate are often not independent, further complicating the interpretation of introgression patterns (Martin and Jiggins 2017). For example, a positive correlation between recombination rate and gene density may lead to higher retention of introgression in gene-dense regions than expected (Schumer et al. 2016; Baker et al. 2017; Schumer et al. 2018; Moran et al. 2021).

Within the protein-coding portion of the genome, introgressed variation should be less common at genes with high divergence or faster rates of adaptive evolution because they are more likely to underlie locally adapted phenotypes or hybrid incompatibilities. However, few empirical studies have tested this prediction. Among modern humans, introgressed Neanderthal ancestry is negatively correlated with fixed differences between humans and Neanderthals, consistent with introgressed variation having negative fitness consequences in high-divergence regions (Vernot and Akey 2014). Conversely, Schumer et al. (2016) found that introgressed loci in *Xiphophorus* swordtails had higher divergence than non-introgressed loci due to reduced selective constraint. Characterizing patterns of introgression across a broader range of taxonomic groups is needed to better understand the factors influencing the distribution of introgression along genomes.

The strongylocentrotid family of sea urchins is a compelling group for characterizing the genomic landscape of introgression. Extensive introgression has occurred among the strongylocentrotid urchins (Glasenapp and Pogson 2023), and the purple sea urchin, *Strongylocentrotus purpuratus* (Stimpson), has a well-annotated reference genome and a long history of use as a model organism in fertilization and development studies. The selective histories of the single-copy protein-coding genes in this family have been formally characterized (Kober and Pogson 2017), providing valuable context for interpreting introgression patterns. The massive effective population sizes of sea urchins should lead to considerably more efficient selection on introgressed variation than most model systems studied thus far. Additionally, their high amounts of recombination (Brennan et al. 2019) and lack of population structure (Palumbi and Wilson 1990; Palumbi and Kessing 1991) should promote the retention of introgressed ancestry. Several studies have documented introgression between a pair of recently-diverged,

non-sister taxa that co-occur and hybridize in both the North Pacific and North Atlantic: *S. pallidus* and *S. droebachiensis* (Addison and Hart 2005; Harper and Hart 2007; Addison and Pogson 2009; Pujolar and Pogson 2011; Glasenapp and Pogson 2023). However, the genomic regions showing signals of introgression have yet to be characterized.

To better understand the fitness consequence of introgression in strongylocentrotid sea urchins, we characterized genomic regions exhibiting introgressed ancestry between *S. pallidus* and *S. droebachiensis* and asked whether these regions show any nonrandom patterns compared to the genome-wide background. We predicted that introgressed regions would have lower gene density, divergence, and rates of evolution than the genome-wide background and that genes with a history of positive selection would show reduced rates of introgression. We further looked for potential cases of adaptive introgression and tested whether introgressed genes were enriched for any gene families or functional categories.

Results

To identify genomic regions supporting introgression between non-sister taxa *S. pallidus* and *S. droebachiensis*, we applied the phylogenetic hidden Markov model PhyloNet-HMM (Liu et al. 2014) to multi-species multiple sequence alignments of the 21 *S. purpuratus* chromosomes, constructed from hard-filtered genotypes of each species in the rooted triplet (*Hemicentrotus pulcherrimus*, (*Strongylocentrotus pallidus*, (*S. droebachiensis*, *S. fragilis*))). PhyloNet-HMM walks along each chromosome, identifies changes in the underlying genealogy, and outputs posterior probabilities of having evolved by each parent tree (i.e., species tree, introgression tree) for each site in the multiple sequence alignment (Liu et al. 2014). The model accounts for both convergence and incomplete lineage sorting (ILS) by employing a finite-sites model and allowing for changes in gene trees within each parent tree (Liu et al. 2014; Liu et al. 2015;

Schumer et al. 2016). We ran PhyloNet-HMM 100 times on each chromosome and averaged the posterior probabilities across runs. To infer introgression tracts, we applied a posterior probability threshold for introgression of 90% and recorded the genomic coordinates of consecutive sites with posterior probabilities at or above this threshold. We also proceeded with a less stringent dataset at the 80% posterior probability threshold for comparison, given the conservative nature of our test (see Discussion) and the small size of the dataset identified at the 90% threshold. In both datasets, the inferred introgression tracts were filtered if they had a mean coverage depth less than 5x or greater than 100x and trimmed if they overlapped a gap of more than 25kb between adjacent genotypes (including invariant sites).

At the 90% posterior probability threshold, we identified 4,855 introgression tracts (≥2 bases) were identified, with 164 exceeding 10kb. Tracts greater than 10kb in length had mean and median lengths of 22,850 and 16,595 base pairs, respectively (Figure 1). The coverage depth and breadth metrics for introgression tracts were similar to the genome-wide averages (Table 1). The percent of bases introgressed, both overall and in coding regions, was 1%.

When the posterior probability threshold was lowered to 80%, the total number of tracts increased to 17,037, with 953 exceeding 10kb. The mean and median tract lengths for 10kb tracts (22,897, 17,236 base pairs) remained similar to those at the 90% threshold. The percentage of bases introgressed rose to 5% overall and 6% in coding regions. These estimates of the proportion of the genome introgressed (1 - 5 %) align with previous estimates for *S. pallidus* and *S. droebachiensis* (Glasenapp and Pogson 2023). Summary statistics for the introgression tracts at both probability thresholds are provided in Supplementary Table S2, and information on all introgression tracts can be found in Supplementary Tables S3 and S4. Additionally, Figure 2 and

Supplementary Figure S1 depict the locations of the 10 kb introgression tracts along chromosomes.

There was a significantly negative association between the percent chromosome introgressed and chromosome gene density (Supplementary Figure S2). The chromosome with the highest percent introgressed and most 10kb introgression tracts (NW_022145606.1) also had the lowest gene density (Supplementary Table S5). Unexpectedly, two chromosomes (NW_022145615.1, NW_022145595.1) did not have any sites that crossed the 90% posterior probability threshold for introgression (Supplementary Table S5). There were no discernible features of these two chromosomes that would lead to reduced power to detect introgression. Both had high site density (Supplementary Table S5), and although NW_022145595.1 is the shortest chromosome at 30 Mb, fifteen of the 21 chromosomes were between 30 and 40 Mb in length. To determine the probability of having two chromosomes without 10 kb introgression tracts due to chance, we divided the genome into non-overlapping 10kb blocks and selected 164 blocks at random 10,000 times, recording the frequency of one or more chromosomes not being represented. The number of times a single chromosome was not represented was 154 in 10,000 (0.015). The number of times two chromosomes were not represented was 1 in 10,000 (0.0001). At the 80% posterior probability threshold, all chromosomes had 10kb introgression tracts, ranging from 9-127 (Supplementary Table S6). Consistent with the results at the 90% threshold level, chromosomes NW_022145615.1 and NW_022145595.1 had the fewest percent of introgressed sites (1.4%, 1.5%) and 10kb introgression tracts (9, 10), while chromosome NW_022145606.1 again had the highest proportion of introgressed sites (11.5%) and the most 10kb introgression tracts (127) (Supplementary Table S6).

To characterize the properties of genomic regions spanned by introgression tracts, we compared estimates of the nucleotide divergence, gene density, coding base density, and rates of evolution for the set of introgressed intervals and genes to null distributions representative of the non-introgressed genome-wide background. For introgression tracts, we generated distributions of average *H. pulcherrimus* - *S. fragilis* absolute nucleotide divergence (d_{XY}), number of overlapping protein-coding genes, number of overlapping coding bases, and number of overlapping genes with a history of positive selection by bootstrap resampling the 10kb introgression tracts with replacement 1,000 times. We compared these distributions to null distributions created by randomly permuting intervals of the same number and size as the introgression tracts into the genomic regions confidently called for the species tree. We found that introgressed regions had significantly lower divergence (d_{XY}) than the genome-wide background (Table 2, Supplementary Figure S3) and overlapped significantly fewer protein-coding genes (Table 2, Supplementary Figure S4), coding bases (Table 2, Supplementary Figure S5), and genes with a history of positive selection (Table 2). To test for differences in rates of evolution between introgressed and non-introgressed genes, we calculated the rate of synonymous substitutions (d_S), nonsynonymous substitutions (d_N), and the ratio of nonsynonymous to synonymous substitutions (d_N/d_S) between *H. pulcherrimus* and *S. fragilis* for genes with a majority of their bases declared introgressed and compared this distribution to a null distribution of the same number of genes with the majority of their bases declared for the species tree. Introgressed genes had significantly lower d_N, d_S, and d_N/d_S (Table 2, Supplementary Figure S6).

We further identified all genes overlapping introgression tracts at both posterior probability thresholds (Supplementary Table S7, S8) using gene models from the latest *S.*

purpuratus genome assembly (Spur_5.0). At the 90% posterior probability threshold, 50 protein-coding genes had all their bases declared introgressed, and another 102 had the majority of their bases introgressed. A total of 2,055 genes overlapped an introgression tract by at least two bases. One noteworthy pattern was that many different hyalin genes had bases declared introgressed. Hyalin, an extracellular matrix glycoprotein, is the major component of the hyaline layer, an extraembryonic matrix serving as a cell adhesion substrate during development (McClay and Fink 1982; Wessel et al. 1998). At the 90% threshold, five unique hyalin genes had bases introgressed (LOC578156, LOC752152, LOC373362, LOC100891695, LOC100891850), and an additional four hyalin genes showed introgression at the 80% threshold (LOC578713, LOC586885, LOC576524, LOC578967). Coverage depth for all but one of these genes (LOC578967) was in the range expected if they were single-copy across the four species analyzed (Supplementary Table S9). The high number of hyalin genes observed may not be unexpected, given that there are 21 hyalin genes in the *S. purpuratus* assembly. To test whether there were more occurrences of hyalin than expected by chance, we randomly sampled the same number of genes as the number of introgressed genes from the set of all genes on the 21 chromosomes 1,000 times and recorded the number of hyalin occurrences. There were 3.3x more hyalin genes in the introgressed set than expected due to chance at the 90% threshold (95% confidence interval: 1.4 - 1.6) and 1.8x at the 80% threshold (95% confidence interval: 4.9 - 5.2). More occurrences of hyalin may be expected than due to random chance if the hyalin genes are clustered near each other on chromosomes and do not segregate independently. However, the introgressed hyalin genes have nonoverlapping coordinates and occur across six different chromosomes, with the shortest gap between genes sharing a chromosome being > 400kb. Furthermore, in no case did a single introgression tract overlap more than one hyalin gene.

To identify other potential examples of adaptive introgression, we looked for overlap between genes with introgressed coding bases and the 1,008 strongylocentrotid single-copy orthologs with a history of positive selection previously identified by Kober and Pogson (2017). The positively selected genes (PSGs) had been previously identified by comparing the codon sites models M7 (Beta) vs. M8 (Beta plus ω) (Yang et al. 2000) using the software CODEML of the PAML Package (Yang, 2007). Branch-sites tests of positive selection were also used to identify lineage-specific episodes of adaptive evolution (Kober and Pogson 2017). At the 90% confidence level, three genes with significant sites tests across the family had the majority of their coding bases declared introgressed, arachidonate 5-lipoxygenase (Figure 3), helicase domino, and kinesin-II 95 kDa subunit (Table 3, Supplementary Table S10). There were 32 PSGs (3.2%) with at least 10% of their coding bases introgressed. At the 80% posterior probability threshold, there was a total of 24 PSGs (2.4%) with the majority of their coding bases declared introgressed (Supplementary Table S11), including six genes that had all their coding bases declared introgressed: arachidonate 5-lipoxygenase, 5-hydroxytryptamine receptor 6, transcription termination factor 1, MAK16 homolog, glutathione peroxidase-like, and 2',3'-cyclic-nucleotide 3'-phosphodiesterase-like (Table 3). The maximum likelihood gene trees for all introgressed PSGs shown in Table 3 grouped *S. pallidus* and *S. droebachiensis* as sister taxa, except for glutathione peroxidase-like, which did not have enough high-quality variant sites for gene tree reconstruction. All candidate introgressed PSGs had high coverage depth in the range expected for single-copy orthologs, indicating that genotyping error likely did not contribute to the introgression signal (Table 3).

We also looked for overlap between introgressed genes and genes with significant branch-sites tests on the *S. pallidus* and *S. droebachiensis* terminal branches, indicating lineage-

specific episodes of adaptive protein evolution (Yang 2005; Zhang et al. 2005). Four genes with significant branch-sites tests on the *S. pallidus* terminal branch had an appreciable proportion of their coding bases introgressed at the 90% posterior probability threshold: kremen protein 1, arylsulfatase, sodium- and chloride-dependent neutral and basic amino acid transporter B(0+), and fibrosurfin-like (Table 4). Two genes with significant branch-sites test on the *S. droebachiensis* terminal branch had coding bases introgressed at the 90% threshold, PHD finger protein 8, and structural maintenance of chromosomes 1A (Table 4). All introgressed genes with significant branch-sites tests in Table 4 supported an *S. pallidus* and *S. droebachiensis* sister relationship with an average bootstrap support of 85%. Additional genes with significant branch-sites tests and introgressed bases are available in Supplementary Table S12-S15.

To determine whether any additional classes of genes were over- or underrepresented in the introgressed set, we tested the genes with a majority of their bases introgressed at the 80% posterior probability threshold for gene ontology enrichment using PANTHER18.0 (Mi et al. 2019; Thomas et al. 2022). Only two significant terms remained after applying a false discovery rate (FDR) correction of 5%. There was an under-enrichment of the cellular component terms “plasma membrane” (GO:0005886, $p = 0.014$) and “cell periphery” (GO:0071944, $p = 0.002$). Interestingly, the cellular component term “membrane” (GO:0016020) was enriched in the set of genes with histories of positive selection from Kober and Pogson (2017). Furthermore, the molecular function term “calcium ion binding” (GO:0005509) and biological process term “proteolysis” (GO:0006508) were overrepresented in the set of positively selected genes (Kober and Pogson 2017) and underrepresented in the collection of introgressed genes, though not significant after correction.

Discussion

Here, we characterized the genomic landscape of introgression between two sea urchin species to gain insight into the factors determining the fate of introgressed variation and the behavior of selection following introgression. Our study is the first to perform local ancestry inference with whole-genome sequencing data in a high gene flow marine invertebrate group. The strongylocentrotid sea urchin family stands out relative to other population genetic models for their massive effective population sizes, highly efficient selection, and high gene flow across ocean basins. Although the species are well-diverged (4.2 - 19.0 mya), and natural hybrids are rare, many of the species show strong signals of historical introgression (Glasenapp and Pogson 2023). In our analysis of introgression between *S. pallidus* and *S. droebachiensis*, we found strong evidence for genome-wide selection against introgression, including two chromosomes depleted of introgression warranting further examination. Although our results suggest that slowly evolving loci with low divergence are more likely to be able to move between species, introgression has also likely been an important source of adaptive genetic variation. Between 1% and 6% of coding bases supported introgression, and numerous genes with histories of positive selection also had a significant number of introgressed coding bases. A handful of the introgressed genes with histories of selection are involved in defense, including arachidonate 5-lipoxygenase, glutathione peroxidase, and toll-like receptor 3. Additionally, the introgression of many hyalin genes distributed across multiple chromosomes suggests potential functional and adaptive significance, possibly related to defense. Hyalin is a large glycoprotein and a major component of the hyaline layer, the egg extracellular matrix that serves as a cell adhesion substrate during gastrulation (McClay and Fink 1982; Adelson and Humphreys 1988; Wessel et

al. 1998). Kober and Pogson (2017) have suggested that the prevalence of positive selection at membrane or extracellular proteins (such as collagens) might be driven by pathogen defense.

Our results were consistent with theoretical predictions about where introgressed ancestry is most likely to be retained in the genome. Introgression was more common in genomic regions expected to be under weaker selection, evidenced by introgressed regions having lower gene density, reduced divergence, slower rates of evolution, and fewer positively selected genes than the non-introgressed genome-wide background. We find it unlikely that these patterns were driven by increased power to detect introgression in low divergence regions, as PhyloNet–HMM requires sequence divergence to detect introgression (Schumer et al. 2016). Furthermore, a negative correlation between introgressed ancestry and sequence divergence has been observed in humans (Vernot and Akey 2014), and many studies have found depleted introgression in functional regions (Teeter et al. 2008; Sankararaman et al. 2014; Janoušek et al. 2015; Juric et al. 2016; Sankararaman et al. 2016; Schumer et al. 2016; Maxwell et al. 2018; Petr et al. 2019). Reduced introgression in regions with high divergence or functional density is likely explained by divergent regions harboring loci underlying local adaptation or Dobzhansky-Muller incompatibilities (Moran et al. 2021). Unfortunately, limited information about natural hybrids and ecological selection in the strongylocentrotid family precludes distinguishing between the different sources of selection against introgressed variation.

Our findings are at odds with those of Schumer et al. (2016), who characterized introgressed *Xiphophorus cortezi* ancestry in *X. nezahualcoyotl* genomes and found that introgressed regions had higher sequence divergence, gene density, and rates of synonymous and nonsynonymous substitutions than the genome-wide background. They demonstrated that the higher divergence of introgressed regions was likely driven by introgression at genes not under

strong selective constraint, which is still consistent with genome-wide selection against introgression. The unique results in the *Xiphophorus* system may be driven by the fact that recombination hotspots are concentrated near promoter-like features in swordtails and occur further from transcription start sites in humans and other species with PRDM9-direction recombination (Myers et al. 2005; Coop et al. 2008; Baker et al. 2017; Moran et al. 2021). Furthermore, the *X. nezahualcoyotl* swordtail genome samples had low genetic diversity ($\theta\pi$: 0.00025 - 0.00082), indicating that low or fluctuating effective population sizes and less efficient selection could have also contributed to the higher-than-expected amount of introgression in gene dense regions. The differences between our findings and those of Schumer et al. (2016) highlight the importance of characterizing admixture and introgression across more taxonomic groups.

Our estimates of the amount of introgression were likely conservative for several reasons. First, introgression between *S. pallidus* and *S. droebachiensis* is likely historical, making it harder to detect because recombination breaks introgressed haplotypes into progressively shorter tracts over time, and new mutations obscure the history of introgression. Most of the strongylocentrotid genes that showed introgression were not fully introgressed, especially those with histories of positive selection. Instead, many genes had one or more small regions with very strong support for introgression. Due to the old age of introgression and the high expected amount of recombination in strongylocentrotid urchins, the scale of introgression is likely at the exon level rather than the whole gene level. Detecting introgressed regions at this small scale is a major challenge for any statistical method, given the limited number of variants in an individual exon. Second, randomly resolving heterozygous sites to create multiple sequence alignments causes switching between maternal and paternal chromosomes, fragmenting introgressed

haplotypes that are heterozygous in our samples and biasing our detection towards introgressed variation that has been fixed. When an introgression tract is heterozygous for ancestry, switching between introgressed and non-introgressed ancestry may lead to ambiguous posterior probabilities (Schumer et al. 2016). For this reason, the introgression tracts we detected are likely fixed and old. Finally, the posterior probabilities of introgression used were likely conservative because we averaged them across 100 independent model runs. For example, for a given site, if 99 of the 100 model runs returned a posterior probability of introgression of 90%, but one run returned a probability of 50%, the average probability of introgression for that site would be 89.6%, not high enough to clear the 90% threshold.

Theory predicts a positive correlation between the extent of introgression and the local recombination rate (Veller et al. 2023). Unfortunately, information on recombination in the strongylocentrotid sea urchins is extremely limited, preventing us from testing this relationship. An outstanding question remains whether differences in recombination rates drove the differences in introgression among the different strongylocentrotid chromosomes. If the number of crossovers per meiosis is constant among chromosomes, shorter chromosomes should have higher per-base recombination rates and retain more introgressed variation. However, we did not find a significant relationship between introgression and chromosome length, and the smallest chromosome had the least amount of introgression, which is inconsistent with expectations.

Without polymorphism data for *S. pallidus* and *S. droebachiensis*, we can only speculate about the proportion of introgression tracts driven to fixation by positive selection. However, selection is expected to be very efficient in these sea urchin species. For example, it was conservatively estimated that 15% of strongylocentrotid single-copy orthologs had experienced positive selection (Kober and Pogson 2017), and *S. purpuratus* shows selection on preferred

usage of synonymous codons (Kober and Pogson 2013). Furthermore, the introgression tracts documented in this study are likely historical and fixed. *S. pallidus* and *S. droebachiensis* diverged 5.3 - 7.6 million years ago (Kober and Bernardi 2013), and natural hybrids between the two are rarely observed (Vasseur 1952). Given the likely old age of introgression, the high expected efficiency of selection, and our bias toward detecting high-frequency variants, it is not unreasonable to assume that a small proportion of the introgression tracts spanning coding regions contained advantageous mutations. Future studies will test for recent selection at the genomic intervals inferred to have been introgressed.

In summary, our study documented strong evidence for genome-wide selection against introgressed variation, suggesting that slowly evolving, low-divergence genomic regions are more likely to move between species and avoid negative selection following hybridization and introgression. However, despite strong selection against introgression, we also identified numerous candidate adaptively introgressed genes, indicating that introgression has been an important source of adaptive genetic variation. The strongylocentrotid sea urchin family represents a valuable model system for further characterization of introgression given the high amount of gene flow and genetic diversity among the different species.

Materials and Methods

Study System

Four species forming a rooted triplet were used in the present study: (*Hemicentrotus pulcherrimus*, (*Strongylocentrotus pallidus*, (*S. droebachiensis*, and *S. fragilis*))). The metadata for the sample accessions are presented in Supplementary Table S1. The three Strongylocentrotus taxa were sampled from the East Pacific: *S. droebachiensis* and *S. pallidus* were dredged from Friday Harbor, WA, and *S. fragilis* was collected in Monterey Bay. *H. pulcherrimus* was chosen as the outgroup as it was sampled from the West Pacific (coastal Japan by Y. Agatsuma) and diverged from the *Strongylocentrotus* taxa 10 – 14 mya (Kober and Bernardi 2013). *S. pallidus* and *S. droebachiensis* have broad, overlapping Holarctic distributions with ample opportunity for hybridization. They co-occur in the West Pacific, East Pacific, Arctic, West Atlantic, and East Atlantic Oceans. The geographic history of speciation is challenging to interpret, but fossil evidence confirms that both species speciated in the Pacific and crossed the Bering Sea in the late Miocene to colonize the Arctic and Atlantic Oceans (Durham and MacNeil 1967). Both species show little differentiation between the Pacific and Atlantic due to high trans-Arctic gene flow (Palumbi and Kessing 1991; Addison and Hart 2005; Addison and Kim 2022).

The eggs of *S. droebachiensis* are highly susceptible to fertilization by heterospecific sperm (Strathmann 1981; Levitan 2002), and hybrid matings readily occur when spawning *S. droebachiensis* females are closer to heterospecific males than conspecific males (Levitan 2002). Hybrids between *S. pallidus* and *S. droebachiensis* have also been successfully reared and backcrossed in the lab (Strathmann 1981). Although reproductive isolation between *S. pallidus*

and *S. droebachiensis* appears incomplete, the two species remain distinct across their overlapping ranges (Vasseur 1952; Strathmann 1981). However, hybrids of *S. pallidus* and *S. droebachiensis* morphologically resemble *S. pallidus* as larvae and *S. droebachiensis* as adults, so the frequency of natural hybrids may be underestimated. Introgression between *S. pallidus* and *S. droebachiensis* has been previously detected (Addison and Hart 2005; Harper et al. 2007; Addison and Pogson 2009; Pujolar and Pogson 2011; Glasenapp and Pogson 2023).

Data Pre-Processing

A single genome from each strongylocentrotid species had been previously sequenced on the Illumina HiSeq 2500 (Kober and Bernardi 2013; Kober and Pogson 2017). The raw sequencing reads were pre-processed following GATK's Best Practices (Van der Auwera et al. 2013). Briefly, adapters were marked with Picard MarkIlluminaAdapters, and sequencing reads were mapped to the *S. purpuratus* reference genome (Spur_5.0) with bwa-mem2 v2.2.1 (Vasimuddin et al. 2019). Duplicates were marked with Picard MarkDuplicates, and reference mapping was evaluated using samtools flagstat (Danecek et al. 2021) and mosdepth v0.3.3 (Pedersen and Quinlan 2018). Variant calling and joint genotyping were performed with GAKT's HaplotypeCaller and GenotypeGVCFs. Variants were hard-filtered for skewed values across all samples following GATK recommendations (Caetano-Anolles 2023). Further filtering was done for genotypes with low-quality scores (GQ<20) and low read depth (DP<3), and single nucleotide variants (SNVs) within three base pairs of an indel were excluded.

PhyloNet-HMM

PhyloNet-HMM (Liu et al. 2014) was used to identify genomic regions supporting introgression between *S. pallidus* and *S. droebachiensis*. PhyloNet-HMM is a hidden Markov model that detects breakpoints between regions supporting different phylogenetic relationships,

accounting for incomplete lineage sorting (ILS) by allowing for changes in gene trees within both the species and introgression trees (Liu et al. 2014; Schumer et al. 2016). PhyloNet-HMM walks across each chromosome, locates changes in the underlying genealogy, and outputs posterior probabilities for each SNV site, reflecting the likelihood that the site evolved along the species and introgression trees. PhyloNet-HMM has been used to detect introgressed regions in swordtails (Schumer et al. 2016; Powell et al. 2020), house mouse (Liu et al. 2015), North American admiral butterfly (Mullen et al. 2020), *Danaus* butterfly (Aardema and Andolfatto 2016), and snowshoe hare (Jones et al. 2020) genomes. (Schumer et al. 2016)) conducted performance tests of PhyloNet-HMM on simulated swordtail data and concluded that the approach could accurately distinguish between ILS sorting and hybridization.

Multiple sequence alignments of variant sites were created for each of the 21 *S. purpuratus* chromosomes using vcf2phylip (Ortiz 2019). The 21 chromosomes represent 90% of the S. purpuratus reference genome bases. Although it is known that *S. purpuratus* has a genetically based sex determination, the sex chromosomes have yet to be identified (Pieplow et al. 2023). PhyloNet-HMM only allows for DNA base characters in the input sequence alignments, so all indels were excluded, and only variable sites where all four samples had genotypes passing filter were used. Heterozygous genotypes were randomly resolved because PhyloNet-HMM does not support IUPAC ambiguity codes, and accurate phasing could not be performed across entire chromosomes with a single diploid genome per species and no reference panel (Bukowicki et al. 2016). We ran PhyloNet-HMM on each chromosome 100 times using the default settings to avoid the effects of reaching local optima during hill climbing and averaged the posterior probabilities across independent runs. The average distance between variable sites

in the alignments was 85 base pairs. The multiple sequence alignments including invariant sites had 2,361 gaps greater than 25 kb in length, with the largest gap being 585,224 base pairs.

We used two different posterior probability thresholds to identify introgression tracts: 90% and 80%. Introgression tracts were inferred by recording the genomic coordinates of consecutive sites with posterior probabilities at or above the threshold. The mean coverage depth for each introgression tract for each species was calculated with mosdepth (Pedersen and Quinlan 2018), and introgression tracts where any species had coverage depth less than 5x or greater than 100x were excluded. Introgression tracts overlapping a gap of 25 kb or more between adjacent genotypes (including invariant sites) were identified using bedtools intersect (Quinlan and Hall 2010) and trimmed to remove the gap. Coverage depth metrics were estimated for all introgression tracts passing filter using mosdepth (Pedersen and Quinlan 2018). For each introgression tract, overlapping genes and coding bases were recorded using the gff file from the *S. purpuratus* assembly and bedtools intersect (Quinlan and Hall 2010). We also intersected the introgression tracts with the set of genes with a history of positive selection within the strongylocentrotid family identified by (Kober and Pogson 2017).

Properties of Introgressed Regions

To characterize the genomic landscape of introgression, we compared nucleotide divergence, gene density, coding base density, and rates of evolution between the set of introgressed intervals greater than 10 kb in length to null distributions representative of the non-introgressed genome-wide background (i.e., species tree regions). To create a null distribution of intervals, we created 1,000 replicate interval sets by randomly permuting intervals of the same number and size of the 10kb introgression tracts into regions confidently called for the species tree using bedtools shuffle (Quinlan and Hall 2010). To create a null distribution of non-

introgressed genes, we created 1,000 replicates of random genes (the same length as the number of introgressed genes) with the majority of their bases confidently called for the species tree.

Divergence

We compared mean absolute nucleotide divergence (d_{XY}) between *S. fragilis* and *H. pulcherrimus* for introgressed and non-introgressed genomic regions. These two species were chosen because they have experienced no or minimal introgression, and introgression between *S. pallidus* and *S. droebachiensis* in either direction should not affect sequence divergence between *S. fragilis* and *H. pulcherrimus*. The two species involved in introgression (*S. pallidus*, *S. droebachiensis*) were not included in the divergence measures because introgression from *S. droebachiensis* into *S. pallidus* would decrease *S. fragilis* - *S. pallidus* divergence, introgression from *S. pallidus* into *S. droebachiensis* would decrease *S. fragilis* - *S. droebachiensis* divergence, and introgression between *S. pallidus* and *S. droebachiensis* in either direction would reduce *S. pallidus* - *S. droebachiensis* divergence (see Forsythe et al. 2020).

To get distributions of d_{XY}, we first generated a new genotype (vcf) file for *S. fragilis* and *H. pulcherrimus*, including invariant sites. Vcf files typically only contain variant sites, and d_{XY} estimates can be downwardly biased by assuming missing sites are invariant (Korunes and Samuk 2021). We generated the new genotype file by combining the single sample vcf files for *H. pulcherrimus* and *S. fragilis* and performing joint genotyping using GATK's GenotypeGVCFs with the –include-non-variant-sites option. Variant and invariant sites were then split into separate files for filtering. Variant sites were hard-filtered for skewed values across all samples following GATK recommendations (Caetano-Anolles 2023). The variant and invariant site vcf files were then merged back together, and genotypes with low-quality scores

(GQ<30), low read depth (DP<8), or low reference genotype confidence (RGQ<30) were set to missing.

We used pixy (Korunes and Samuk 2021) to calculate d_{XY} for each introgression tract greater than 10 kb. To generate a distribution of mean d_{XY} values, we bootstrap resampled the introgression tracts and their d_{XY} values with replacement to generate 1,000 pseudoreplicate datasets and calculated the mean d_{XY} for each. To generate a null distribution of mean d_{XY} values representative of the non-introgressed genome-wide background, we calculated mean d_{XY} for the 1,000 replicate sets of null intervals. The distributions of mean d_{XY} for introgression and species tree tracts were then compared using a two-sided, two-sample Welch's t-test.

Gene Density

To determine whether introgressed regions were more or less likely to overlap protein-coding genes and bases than the genome-wide background, we bootstrap resampled the introgression tracts with replacement to create 1,000 pseudoreplicate datasets and counted the number of overlapping coding bases and the number of protein-coding genes with at least 50% of their bases declared introgressed. The same process was repeated for genes with a history of positive selection from (Kober and Pogson 2017). We identified the overlapping genes and coding bases by intersecting the introgression tract interval files with the protein-coding gene and CDS coordinates for *S. purpuratus* using bedtools intersect. To standardize the protein-coding gene counts, we divided the values by the total length of the interval files in megabases. To normalize the coding base counts, we estimated the percentage of bases that were coding in each pseudoreplicate interval file. To generate null distributions for protein-coding genes and coding base counts, we used the same procedure to count the number of overlapping coding bases and protein-coding genes in the 1,000 replicate sets of null intervals.

Rate of Evolution

To compare the rate of evolution between introgressed and non-introgressed genes, we generated distributions of the rate of nonsynonymous substitutions (d_N), the rate of synonymous substitutions (d_S), and the ratio of the rates of nonsynonymous to synonymous substitutions (d_N/d_S) using model M0 in the CODEML program of the PAML package (Yang 2007). We first identified genes with greater than 50% of their bases declared introgressed at each posterior probability threshold, excluding those with mean coverage depth less than 10x or greater than 100x, or with fewer than 75% of their coding bases covered by one read or fewer than 50% by ten reads. We created sequence alignments of *S. fragilis* and *H. pulcherrimus* for each introgressed gene passing filter using vcf2fasta and estimated d_N, d_S, and d_N/d_S using CODEML. We specified the cleandata=1 option to remove sites with ambiguity data. We generated distributions for d_N, d_S, and d_N/d_S by bootstrap resampling the introgressed genes and their values with replacement 1,000 times and calculating mean d_N, d_S, and d_N/d_S. To generate null distributions for d_N, d_S, and d_N/d_S, we estimated d_N, d_S, and d_N/d_S for all putative single-copy protein-coding genes that had the majority of their bases confidently called for the species tree, filtered by the same metrics as the introgressed genes. We then randomly sampled the list of genes and their d_N, d_S, and d_N/d_S values without replacement to create 1,000 replicate gene lists of the same size as the number of introgressed genes and calculated mean d_N, d_S, and d_N/d_S.

Data Accessibility and Benefit-Sharing

Data Accessibility Statement

The data and code supporting this study's findings are available on Dryad (https://doi.org/10.5061/dryad.fn2z34v1k). Raw sequence reads are available in the NCBI SRA (BioProject PRJNA391452).

Acknowledgments

Funding for data collection for the study was provided by the National Science Foundation (DEB-1011061), the STEPS Foundation, Friends of Long Marine Lab, and the Myers Trust. The funding bodies did not participate in research design, sample collection, data analysis, or manuscript writing. We thank UC Santa Cruz for access to the Hummingbird computational cluster and Qiqige Wuyun for their help with PhyloNet-HMM. The authors have no conflicts of interest to declare.

References

Aardema ML, Andolfatto P. 2016. Phylogenetic incongruence and the evolutionary origins of cardenolide-resistant forms of Na+,K+-ATPase in *Danaus* butterflies. *Evolution* 70:1913–1921.

Addison JA, Hart MW. 2005. Colonization, dispersal, and hybridization influence phylogeography o North Atlantic sea urchins (*Strongylocentrotus droebachiensis*). *Evolution* 59:532–543.

Addison JA, Kim J. 2022. Trans-Arctic vicariance in *Strongylocentrotus* sea urchins. *PeerJ* 10:e13930.

Addison JA, Pogson GH. 2009. Multiple gene genealogies reveal asymmetrical hybridization and introgression among strongylocentrotid sea urchins. *Mol. Ecol.* 18:1239–1251.

Adelson DL, Humphreys T. 1988. Sea urchin morphogenesis and cell–hyalin adhesion are perturbed by a monoclonal antibody specific for hyalin. *Development* 104:391–402.

Arnegard ME, McGee MD, Matthews B, Marchinko KB, Conte GL, Kabir S, Bedford N, Bergek S, Chan YF, Jones FC, et al. 2014. Genetics of ecological divergence during speciation. *Nature* 511:307–311.

Arnold BJ, Lahner B, DaCosta JM, Weisman CM, Hollister JD, Salt DE, Bomblies K, Yant L. 2016. Borrowed alleles and convergence in serpentine adaptation. *Proc. Natl. Acad. Sci.* 113:8320–8325.

Baker Z, Schumer M, Haba Y, Bashkirova L, Holland C, Rosenthal GG, Przeworski M. 2017. Repeated losses of PRDM9-directed recombination despite the conservation of PRDM9 across vertebrates. *eLife* 6:e24133.

Barton N, Bengtsson BO. 1986. The barrier to genetic exchange between hybridising populations. *Heredity* 57:357–376.

Barton NH. 1983. Multilocus clines. *Evolution* 37:454–471.

Brandvain Y, Kenney AM, Flagel L, Coop G, Sweigart AL. 2014. Speciation and introgression between *Mimulus nasutus* and *Mimulus guttatus*. *PLOS Genet.* 10:e1004410.

Brennan RS, Garrett AD, Huber KE, Hargarten H, Pespeni MH. 2019. Rare genetic variation and balanced polymorphisms are important for survival in global change conditions. *Proc. R. Soc. B Biol. Sci.* 286:20190943.

Bukowicki M, Franssen SU, Schlötterer C. 2016. High rates of phasing errors in highly polymorphic species with low levels of linkage disequilibrium. *Mol. Ecol. Resour.* 16:874–882.

Caetano-Anolles D. 2023. (How to) Filter variants either with VQSR or by hard-filtering. *GATK* [Internet]. Available from: https://gatk.broadinstitute.org/hc/en-us/articles/360035531112--How-to-Filter-variants-either-with-VQSR-or-by-hard-filtering

Calfee E, Gates D, Lorant A, Perkins MT, Coop G, Ross-Ibarra J. 2021. Selective sorting of ancestral introgression in maize and teosinte along an elevational cline. *PLOS Genet.* 17:e1009810.

Coop G, Wen X, Ober C, Pritchard JK, Przeworski M. 2008. High-resolution mapping of crossovers reveals extensive variation in fine-scale recombination patterns among humans. *Science* 319:1395–1398.

Cooper BS, Sedghifar A, Nash WT, Comeault AA, Matute DR. 2018. A maladaptive combination of traits contributes to the maintenance of a *Drosophila* hybrid zone. *Curr. Biol.* 28:2940-2947.e6.

Corbett-Detig R, Nielsen R. 2017. A hidden Markov model approach for simultaneously estimating local ancestry and admixture time using next generation sequence data in samples of arbitrary ploidy. *PLOS Genet.* 13:e1006529.

Danecek P, Bonfield JK, Liddle J, Marshall J, Ohan V, Pollard MO, Whitwham A, Keane T, McCarthy SA, Davies RM, et al. 2021. Twelve years of samtools and bcftools. *GigaScience* 10:giab008.

Durham JW, MacNeil FS. 1967. Cenozoic migrations of marine invertebrates through the Bering Strait region. In: The Bering Land Bridge. Stanford University Press. p. 326–349. Available from: https://www.vliz.be/en/imis

Feng C, Wang J, Liston A, Kang M. 2023. Recombination variation shapes phylogeny and introgression in wild diploid strawberries. *Mol. Biol. Evol.* 40:msad049.

Forsythe ES, Sloan DB, Beilstein MA. 2020. Divergence-based introgression polarization. *Genome Biol. Evol.* 12:463–478.

Glasenapp MR, Pogson GH. 2023. Extensive introgression among strongylocentrotid sea urchins revealed by phylogenomics. *Ecol. Evol.* 13:e10446.

Harper FM, Addison JA, Hart MW. 2007. Introgression versus immigration in hybridizing high-dispersal echinoderms. *Evolution* 61:2410–2418.

Harper FM, Hart MW. 2007. Morphological and phylogenetic evidence for hybridization and introgression in a sea star secondary contact zone: hybridization between *Asterias* sea stars. *Invertebr. Biol.* 126:373–384.

Harris K, Nielsen R. 2016. The genetic cost of Neanderthal introgression. *Genetics* 203:881–891.

Hedrick PW. 2013. Adaptive introgression in animals: examples and comparison to new mutation and standing variation as sources of adaptive variation. *Mol. Ecol.* 22:4606–4618.

Huerta-Sánchez E, Jin X, Asan, Bianba Z, Peter BM, Vinckenbosch N, Liang Y, Yi X, He M, Somel M, et al. 2014. Altitude adaptation in Tibetans caused by introgression of Denisovan-like DNA. *Nature* 512:194–197.

Janoušek V, Munclinger P, Wang L, Teeter KC, Tucker PK. 2015. Functional organization of the genome may shape the species boundary in the house mouse. *Mol. Biol. Evol.* 32:1208–1220.

Jones MR, Mills LS, Jensen JD, Good JM. 2020. The origin and spread of locally adaptive seasonal camouflage in snowshoe hares. 196:271–389.

Juric I, Aeschbacher S, Coop G. 2016. The strength of selection against Neanderthal introgression. *PLOS Genet.* 12:e1006340.

Kim BY, Huber CD, Lohmueller KE. 2018. Deleterious variation shapes the genomic landscape of introgression. *PLOS Genet.* 14:e1007741.

Kober KM, Bernardi G. 2013. Phylogenomics of strongylocentrotid sea urchins. *BMC Evol. Biol.* 13:88.

Kober KM, Pogson GH. 2013. Genome-wide patterns of codon bias are shaped by natural selection in the purple sea urchin, *Strongylocentrotus purpuratus*. *G3 GenesGenomesGenetics* 3:1069–1083.

Kober KM, Pogson GH. 2017. Genome-wide signals of positive selection in strongylocentrotid sea urchins. *BMC Genomics* 18:555.

Korunes KL, Samuk K. 2021. pixy: Unbiased estimation of nucleotide diversity and divergence in the presence of missing data. *Mol. Ecol. Resour.* 21:1359–1368.

Lamichhaney S, Berglund J, Almén MS, Maqbool K, Grabherr M, Martinez-Barrio A, Promerová M, Rubin C-J, Wang C, Zamani N, et al. 2015. Evolution of Darwin's finches and their beaks revealed by genome sequencing. *Nature* 518:371–375.

Levitan DR. 2002. The relationship between conspecific fertilization success and reproductive isolation among three congeneric sea urchins. *Evolution* 56:1599–1689.

Liu KJ, Dai J, Truong K, Song Y, Kohn MH, Nakhleh L. 2014. An HMM-based comparative genomic framework for detecting introgression in eukaryotes. *PLoS Comput. Biol.* 10:e1003649.

Liu KJ, Steinberg E, Yozzo A, Song Y, Kohn MH, Nakhleh L. 2015. Interspecific introgressive origin of genomic diversity in the house mouse. *Proc. Natl. Acad. Sci.* 112:196–201.

Martin SH, Davey JW, Salazar C, Jiggins CD. 2019. Recombination rate variation shapes barriers to introgression across butterfly genomes. *PLOS Biol.* 17:e2006288.

Martin SH, Jiggins CD. 2017. Interpreting the genomic landscape of introgression. *Curr. Opin. Genet. Dev.* 47:69–74.

Maxwell CS, Sepulveda VE, Turissini DA, Goldman WE, Matute DR. 2018. Recent admixture between species of the fungal pathogen *Histoplasma*. *Evol. Lett.* 2:210–220.

McBride CS, Singer MC. 2010. Field studies reveal strong postmating isolation between ecologically divergent butterfly populations. *PLOS Biol.* 8:e1000529.

McClay DR, Fink RD. 1982. Sea urchin hyalin: appearance and function in development. *Dev. Biol.* 92:285–293.

Mi H, Muruganujan A, Huang X, Ebert D, Mills C, Guo X, Thomas PD. 2019. Protocol update for large-scale genome and gene function analysis with the PANTHER classification system (v.14.0). *Nat. Protoc.* 14:703–721.

Moran BM, Payne C, Langdon Q, Powell DL, Brandvain Y, Schumer M. 2021. The genomic consequences of hybridization. *eLife* 10:e69016.

Mullen SP, VanKuren NW, Zhang W, Nallu S, Kristiansen EB, Wuyun Q, Liu K, Hill RI, Briscoe AD, Kronforst MR. 2020. Disentangling population history and character evolution among hybridizing lineages. *Mol. Biol. Evol.* 37:1295–1305.

Myers S, Bottolo L, Freeman C, McVean G, Donnelly P. 2005. A fine-scale map of recombination rates and hotspots across the human genome. *Science* 310:321–324.

Orr HA. 1995. The population genetics of speciation: the evolution of hybrid incompatibilities. *Genetics* 139:1805–1813.

Ortiz EM. 2019. vcf2phylip v2.0: convert a VCF matrix into several matrix formats for phylogenetic analysis. Available from: https://zenodo.org/record/2540861

Palumbi SR, Kessing BD. 1991. Population biology of the trans-arctic exchange: mtDNA sequence similarity between Pacific and Atlantic sea urchins. *Evolution* 45:1790–1805.

Palumbi SR, Wilson AC. 1990. Mitochondrial Dna Diversity in the Sea Urchins Strongylocentrotus Purpuratus and S. Droebachiensis. *Evolution* 44:403–415.

Pedersen BS, Quinlan AR. 2018. Mosdepth: quick coverage calculation for genomes and exomes. *Bioinformatics* 34:867–868.

Petr M, Pääbo S, Kelso J, Vernot B. 2019. Limits of long-term selection against Neandertal introgression. *Proc. Natl. Acad. Sci.* 116:1639–1644.

Pieplow CA, Furze AR, Wessel GM. 2023. A case of hermaphroditism in the gonochoristic sea urchin, *Strongylocentrotus purpuratus*, reveals key mechanisms of sex determination. *Biol. Reprod.* 108:960–973.

Pool JE. 2015. The Mosaic ancestry of the *Drosophila* genetic reference panel and the *D. melanogaster* reference genome reveals a network of epistatic fitness interactions. *Mol. Biol. Evol.* 32:3236–3251.

Powell DL, García-Olazábal M, Keegan M, Reilly P, Du K, Díaz-Loyo AP, Banerjee S, Blakkan D, Reich D, Andolfatto P, et al. 2020. Natural hybridization reveals incompatible alleles that cause melanoma in swordtail fish. *Science* 368:731–736.

Pujolar JM, Pogson GH. 2011. Positive darwinian selection in gamete recognition proteins of *Strongylocentrotus* sea urchins. *Mol. Ecol.* 20:4968–4982.

Quinlan AR, Hall IM. 2010. BEDTools: a flexible suite of utilities for comparing genomic features. *Bioinformatics* 26:841–842.

Ravinet M, Kume M, Ishikawa A, Kitano J. 2021. Patterns of genomic divergence and introgression between Japanese stickleback species with overlapping breeding habitats. *J. Evol. Biol.* 34:114–127.

Ravinet M, Yoshida K, Shigenobu S, Toyoda A, Fujiyama A, Kitano J. 2018. The genomic landscape at a late stage of stickleback speciation: high genomic divergence interspersed by small localized regions of introgression. *PLOS Genet.* 14:e1007358.

Sankararaman S, Mallick S, Dannemann M, Prüfer K, Kelso J, Pääbo S, Patterson N, Reich D. 2014. The genomic landscape of Neanderthal ancestry in present-day humans. *Nature* 507:354–357.

Sankararaman S, Mallick S, Patterson N, Reich D. 2016. The combined landscape of Denisovan and Neanderthal ancestry in present-day humans. *Curr. Biol.* 26:1241–1247.

Schumer M, Cui R, Powell DL, Rosenthal GG, Andolfatto P. 2016. Ancient hybridization and genomic stabilization in a swordtail fish. *Mol. Ecol.* 25:2661–2679.

Song Y, Endepols S, Klemann N, Richter D, Matuschka F-R, Shih C-H, Nachman MW, Kohn MH. 2011. Adaptive introgression of anticoagulant rodent poison resistance by hybridization between Old World mice. *Curr. Biol.* 21:1296–1301.

Strathmann RR. 1981. On barriers to hybridization between *Strongylocentrotus droebachiensis* (O.F. Müller) and *S. pallidus* (G.O. Sars). *J. Exp. Mar. Biol. Ecol.* 55:39–47.

Teeter KC, Payseur BA, Harris LW, Bakewell MA, Thibodeau LM, O'Brien JE, Krenz JG, Sans-Fuentes MA, Nachman MW, Tucker PK. 2008. Genome-wide patterns of gene flow across a house mouse hybrid zone. *Genome Res.* 18:67–76.

The Heliconius Genome Consortium. 2012. Butterfly genome reveals promiscuous exchange of mimicry adaptations among species. *Nature* 487:94–98.

Thomas PD, Ebert D, Muruganujan A, Mushayahama T, Albou L-P, Mi H. 2022. PANTHER: Making genome-scale phylogenetics accessible to all. *Protein Sci.* 31:8–22.

Van der Auwera GA, Carneiro MO, Hartl C, Poplin R, del Angel G, Levy-Moonshine A, Jordan T, Shakir K, Roazen D, Thibault J, et al. 2013. From fastq data to high-confidence variant calls: the genome analysis toolkit best practices pipeline. *Curr. Protoc. Bioinforma.* 43:11.10.1-11.10.33.

Vasimuddin Md, Misra S, Li H, Aluru S. 2019. Efficient architecture-aware acceleration of bwa-mem for multicore systems. In: 2019 IEEE International Parallel and Distributed Processing Symposium (IPDPS). Rio de Janeiro, Brazil: IEEE. p. 314–324. Available from: https://ieeexplore.ieee.org/document/8820962/

Vasseur E. 1952. Geographic variation in the Norwegian sea urchins, *Strongylocentrotus droebachiensis* and *S. pallidus*. *Evolution* 6:87–100.

Veller C, Edelman NB, Muralidhar P, Nowak MA. 2023. Recombination and selection against introgressed DNA. *Evolution* 77:1131–1144.

Vernot B, Akey JM. 2014. Resurrecting surviving Neandertal lineages from modern human genomes. *Science* 343:1017–1021.

Wessel GM, Berg L, Adelson DL, Cannon G, McClay DR. 1998. A molecular analysis of hyalin—a substrate for cell adhesion in the hyaline layer of the sea urchin embryo. *Dev. Biol.* 193:115–126.

Yang Z. 2005. Bayes empirical bayes inference of amino acid sites under positive selection. *Mol. Biol. Evol.* 22:1107–1118.

Yang Z. 2007. PAML 4: phylogenetic analysis by maximum likelihood. *Mol. Biol. Evol.* 24:1586–1591.

Zhang J, Nielsen R, Yang Z. 2005. Evaluation of an improved branch-site likelihood method for detecting positive selection at the molecular level. *Mol. Biol. Evol.* 22:2472–2479.

Tables and Figures

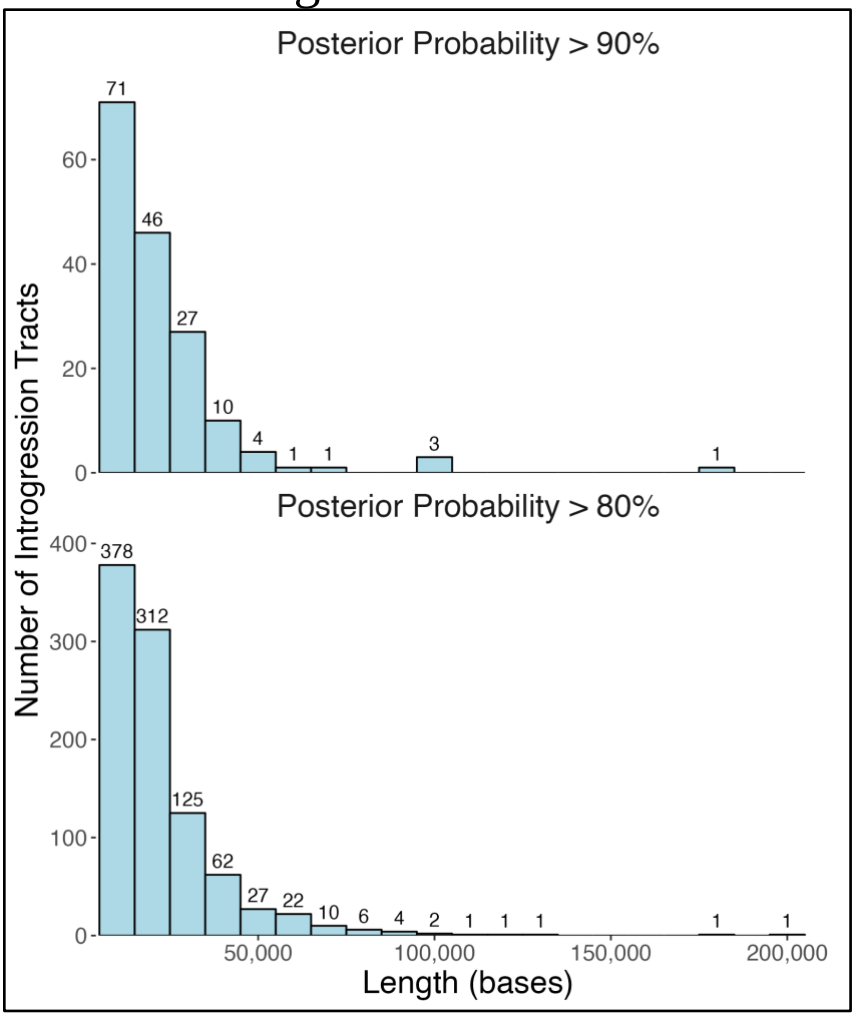

Figure 1. Distribution of introgression tract lengths for introgression tracts greater than 10 kb. Top panel: tract length distribution using a posterior probability cutoff of 90% as evidence of introgression. Bottom panel: tract length distribution using a posterior probability cutoff of 80%.

Table 1. Summary of DNA sequencing and coverage.

Species	**% Bases Covered**				**Mean Coverage Depth**			
	Whole Genome[a]	**Coding[b]**	**Introgression Tracts**		**Whole Genome[c]**	**Coding[d]**	**Introgression Tracts**	
			80%	90%			80%	90%
Sdro	78	95	81	81	24.7x	52.9x	25.1x	25.4x
Sfra	81	95	84	85	32.1x	54.8x	32.7x	32.7x
Spal	78	95	82	82	11.9x	17.3x	13.0x	13.5x
Hpul	69	90	71	71	24.5x	54.2x	24.4x	23.5x

[a]Percentage of bases in the *S. purpuratus* reference genome covered with at least one read.
[b]Percentage of coding bases in the *S. purpuratus* reference genome covered with at least one read.
[c]Mean genome-wide coverage depth of the *S. purpuratus* reference genome
[d]Mean coverage depth for coding sequences in the *S. purpuratus* genome assembly

Species abbreviations: *Sdro* - *S. droebachiensis*; *Sfra* - *S. fragilis*; *Spal* - *S. pallidus*; *Hpul* - *H. pulcherrimus*.

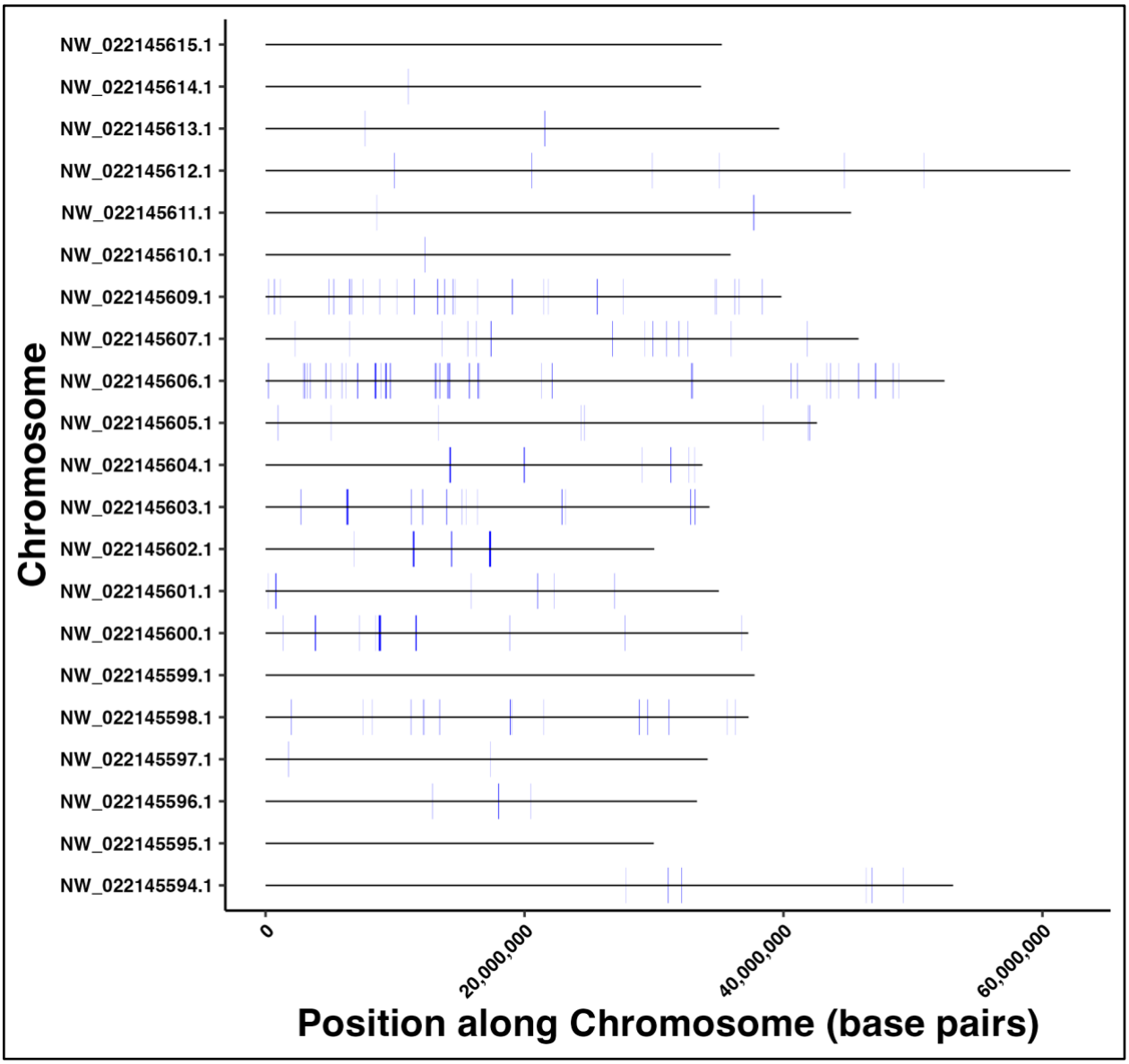

Figure 2. The 164 introgression tracts greater than 10 kb in length by chromosome (posterior probability > 90%). The introgression tracts are displayed as blue rectangles along the chromosomes. The chromosomes are ordered by number (descending).

Table 2. Genomic features of the distribution of 10 kb introgression tracts and the genome-wide background. Means are shown for the introgression tracts. The 95% confidence intervals are shown for the genome-wide background (null distribution). d_{XY}, d_N, d_S, and d_N/d_S.

	d_{XY}	d_N	d_S	d_N/d_S	Genes / Mb	Percent Coding	PSGs[a]/ Mb
Posterior Probability >= 90%							
Introgression Tracts/Genes	0.041	0.013	0.038	0.43	17.6	3.75	0.68
Genome-Wide Background	0.0497 - 0.0499	0.0174 - 0.0175	0.0537 - 0.0538	0.565 - 0.567	28.6 - 28.9	5.18 - 5.24	1.58 - 1.65
Posterior Probability >= 80%							
Introgression Tracts/Genes	0.043	0.013	0.035	0.53	21.3	4.79	.45
Genome-Wide Background	0.050 - 0.051	0.0172 - 0.0173	0.0533 - 0.0533	0.570 - 0.571	28.7 - 28.9	5.24 - 5.26	1.56 - 1.59

[a]Positively Selected Genes: Genes with significant sites tests of positive selection across the strongylocentrotid family.

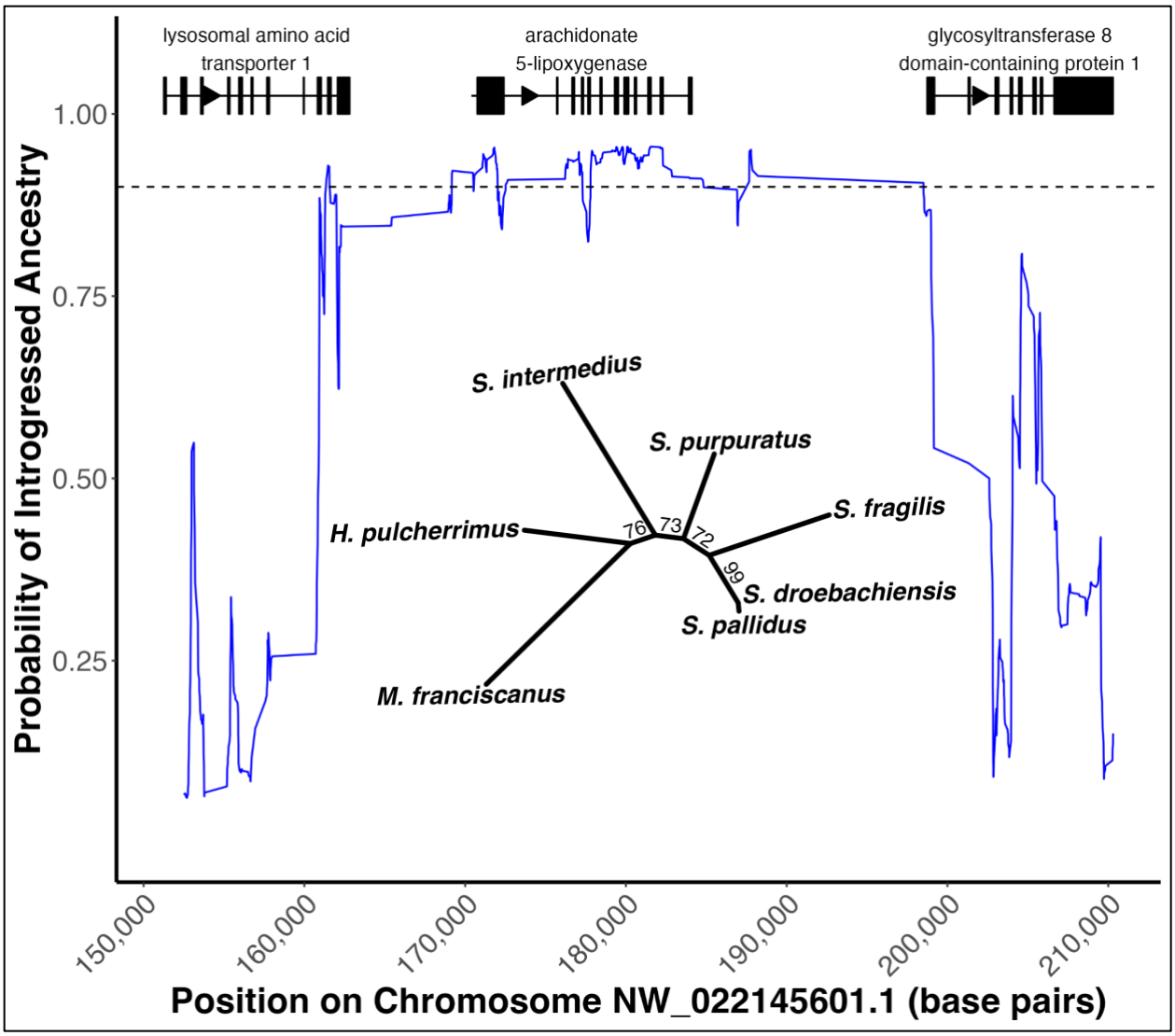

Figure 3. The introgression tract overlapping arachidonate 5-lipoxygenase, a gene with a history of positive selection within the strongylocentrotid sea urchin family. Inside the line plot is the maximum likelihood gene tree for the longest isoform of arachidonate 5-lipoxygenase. Relative to the species tree, the positions of *S. pallidus* and *S. fragilis* are swapped.

Table 3. A selection of genes with a history of positive selection within the strongylocentrotid sea urchin family that overlapped introgression tracts. The list is organized by the percentage of coding bases introgressed at the 90% posterior probability threshold.

Gene Info		**Percent Bases Introgressed**		**Percent Coding Bases Introgressed**		**Spal - Sdro bootstrap[a]**	**Mean Coverage Depth**			
NCBI LOC ID	**Name**	**prob > 0.9**	**prob > 0.8**	**prob > 0.9**	**prob > 0.8**		**Sdro**	**Sfra**	**Spal**	**Hpul**
LOC591845	arachidonate 5-lipoxygenase	92.4	100	71.4	100	100	25.8	33.5	11.9	26.6
LOC764716	helicase domino	52.9	66.3	63.2	79.2	100	34.3	44.9	13.5	56.2
LOC587208	kinesin-II 95 kDa subunit	14.8	36.8	51	61.3	93	32.1	42.3	17.5	24.2
LOC105444929	5-hydroxytryptamine receptor 6	6.1	33	39.6	100	98	45.9	41.2	14.1	45.5
LOC100893326	kremen protein 1*	46.3	60.7	34.9	54.7	82	26	35.9	9.7	19.9
LOC100893626	FAT tumor suppressor homolog 3-like	52	60.9	29.8	40.8	95	28.7	34.9	13	45
LOC100891604	transcription termination factor 1	8.9	66.5	21.8	100	46	22.2	29	7.8	23.5
LOC586606	MAK16 homolog	29.1	100	4.2	100	94	21.7	19.6	8.8	27.7
LOC115921720	glutathione peroxidase-like	0.0	100	0.0	100	n/a[b]	15.2	17.7	6.6	12
LOC115917953	2',3'-cyclic-nucleotide 3'-phosphodiesterase-like	0.0	100	0.0	100	34	18.2	23	6.2	20.4

[a]Bootstrap support for the branch grouping *S. pallidus* and *S. droebachiensis* as sister taxa.
[b]No high-quality variant genotypes were called for this gene despite sufficient coverage.

Species abbreviations: *Sdro*, *S. droebachiensis*; *Sfra*, *S. fragilis*; *Spal*, *S. pallidus*; *Hpul*, *H. pulcherrimus*.

Table 4. Summary of the top genes with introgressed bases that had significant branch-sites tests on either the *S. pallidus* or *S. droebachiensis* terminal branches.

Gene Info		Selective History		Percent Coding Bases Introgressed		Spal - Sdro boot[c]	Mean Coverage Depth			
NCBI LOC ID	**Name**	**PSG[a]**	**Branch[b]**	**prob > 0.9**	**prob > 0.8**		**Sdro**	**Sfra**	**Spal**	**Hpul**
LOC100893326	kremen protein 1	yes	*Spal*	34.9	54.7	82	26	35.9	9.7	19.9
LOC575079	arylsulfatase	yes	*Spal*	18.5	25.7	67	34.3	47.9	17.3	38.2
LOC580597	sodium- and chloride-dependent neutral and basic amino acid transporter B(0+)	yes	*Spal*	14.5	21.1	72	28	28.9	10.8	31.9
LOC590964	fibrosurfin-like	yes	*Spal*	7.1	18.3	100	44.5	51.3	16.3	110.7
LOC105445324	muscarinic acetylcholine receptor M5-like	no	*Spal*	0.0	39.1	87	33.1	33.8	6.2	53.8
eef1g	eukaryotic translation elongation factor 1 gamma	yes	*Spal*	0.0	28.6	89	34.3	35.4	16.8	40.2
LOC577068	prominin 1	yes	*Spal*	0.0	12.3	96	30.7	41.3	16.1	40.2
LOC584837	PHD finger protein 8	no	*Sdro*	20.3	42.8	100	23.2	38.3	9.6	41.7
LOC580943	structural maintenance of chromosomes 1A	yes	*Sdro*	4.3	39.7	59	25	35.7	11.7	37.5
LOC105442321	toll-like receptor 3	no	*Sdro*	0.0	13.3	94	58.1	54.8	18.6	73.7
LOC575208	death-inducer obliterator 1	no	*Sdro*	0.0	10.0	90	41.2	41.8	11.6	46.4

[a]PSG - Positively Selected Gene. A gene with a significant sites tests of positive selection across the strongylocentrotid family.

[b]Branch with significant branch-sites test.

[c]Bootstrap support for the branch grouping *S. pallidus* and *S. droebachiensis* as sister taxa

Species abbreviations: *Sdro*, *S. droebachiensis*; *Sfra*, *S. fragilis*; *Spal*, *S. pallidus*; *Hpul*, *H. pulcherrimus*.

Supplementary Figures

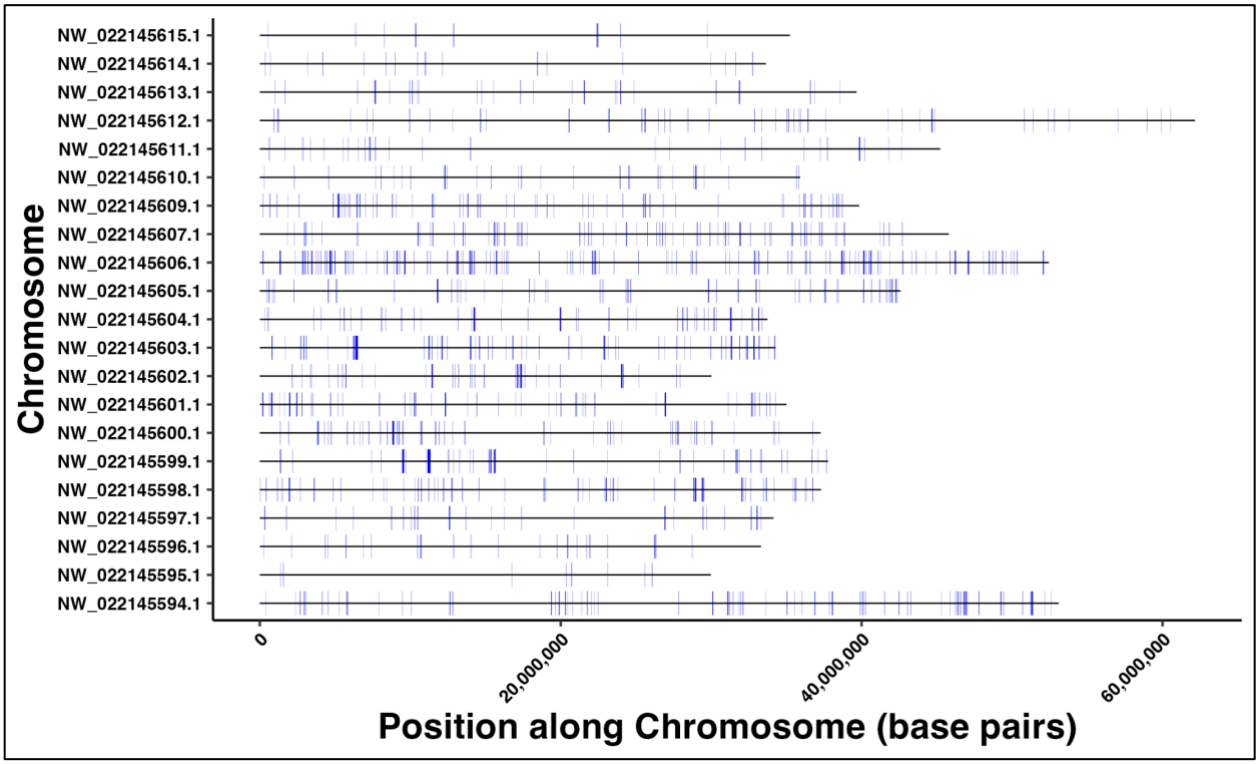

Figure S1. The 953 introgression tracts greater than 10 kb in length by chromosome at the 80% posterior probability threshold. The introgression tracts are displayed as blue rectangles along the chromosomes. The chromosomes are ordered by number (descending).

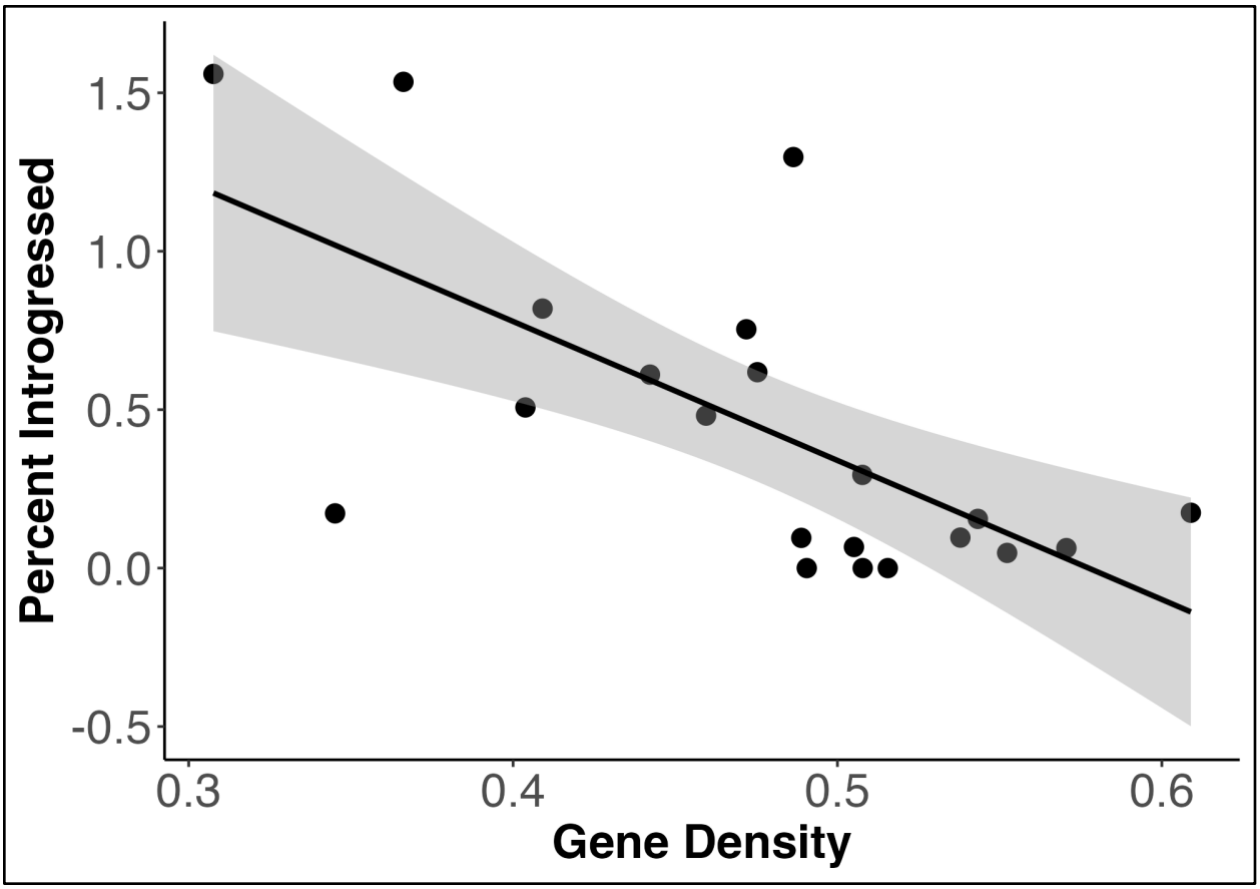

Figure S2. Percent chromosome introgressed by chromosome gene density. Chromosome gene density was calculated as the proportion of bases falling within genic regions (including introns and untranslated regions) for each chromosome. Percent introgressed was calculated as the total length of the 10 kb introgression tracts for each chromosome divided by the total length spanned in the chromosome multiple sequence alignments scanned by PhyloNet-HMM.

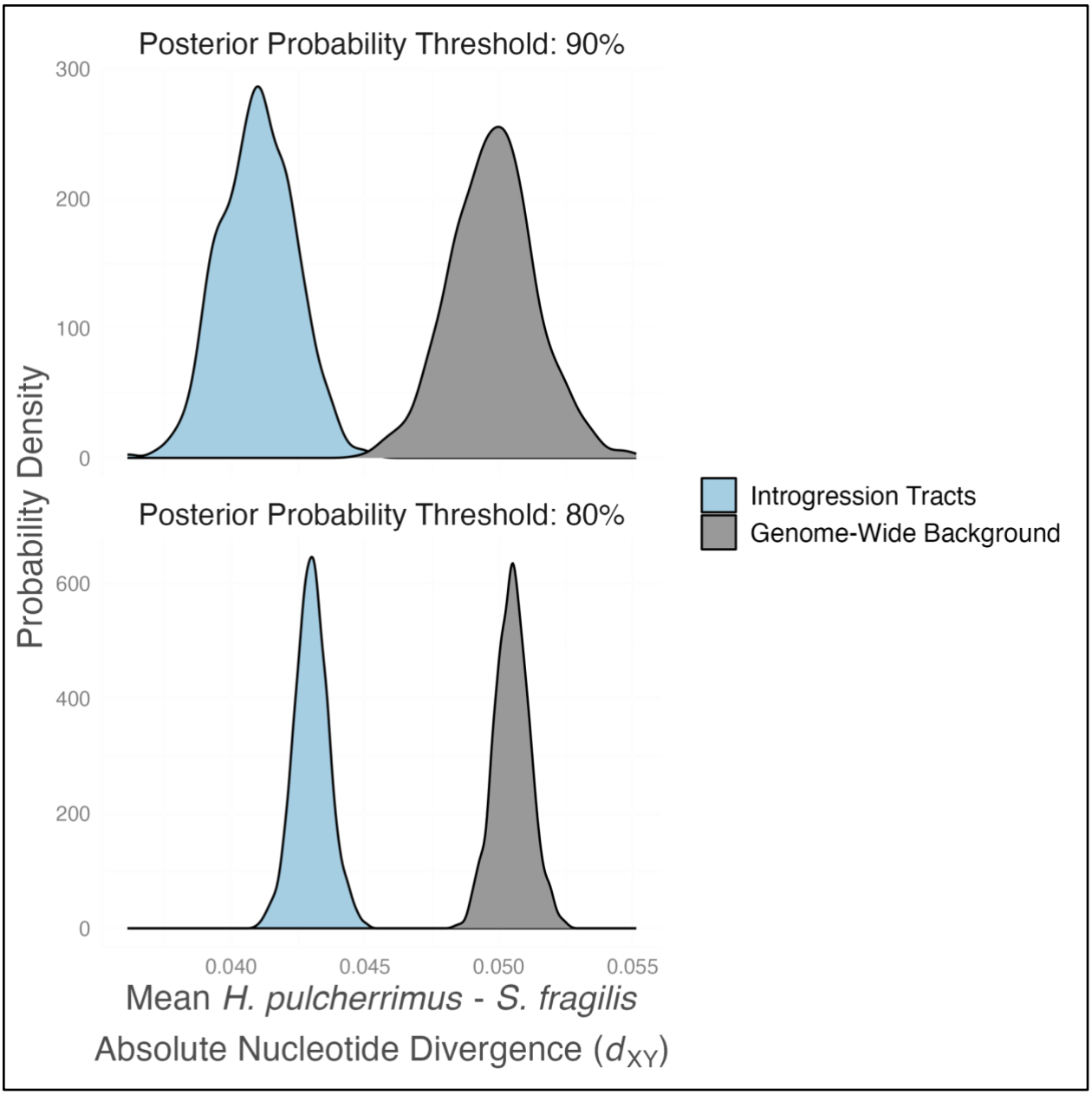

Figure S3. Probability density plot for mean absolute nucleotide divergence (d_{XY}) for introgression tracts greater than 10 kb in length and the genome-wide background.

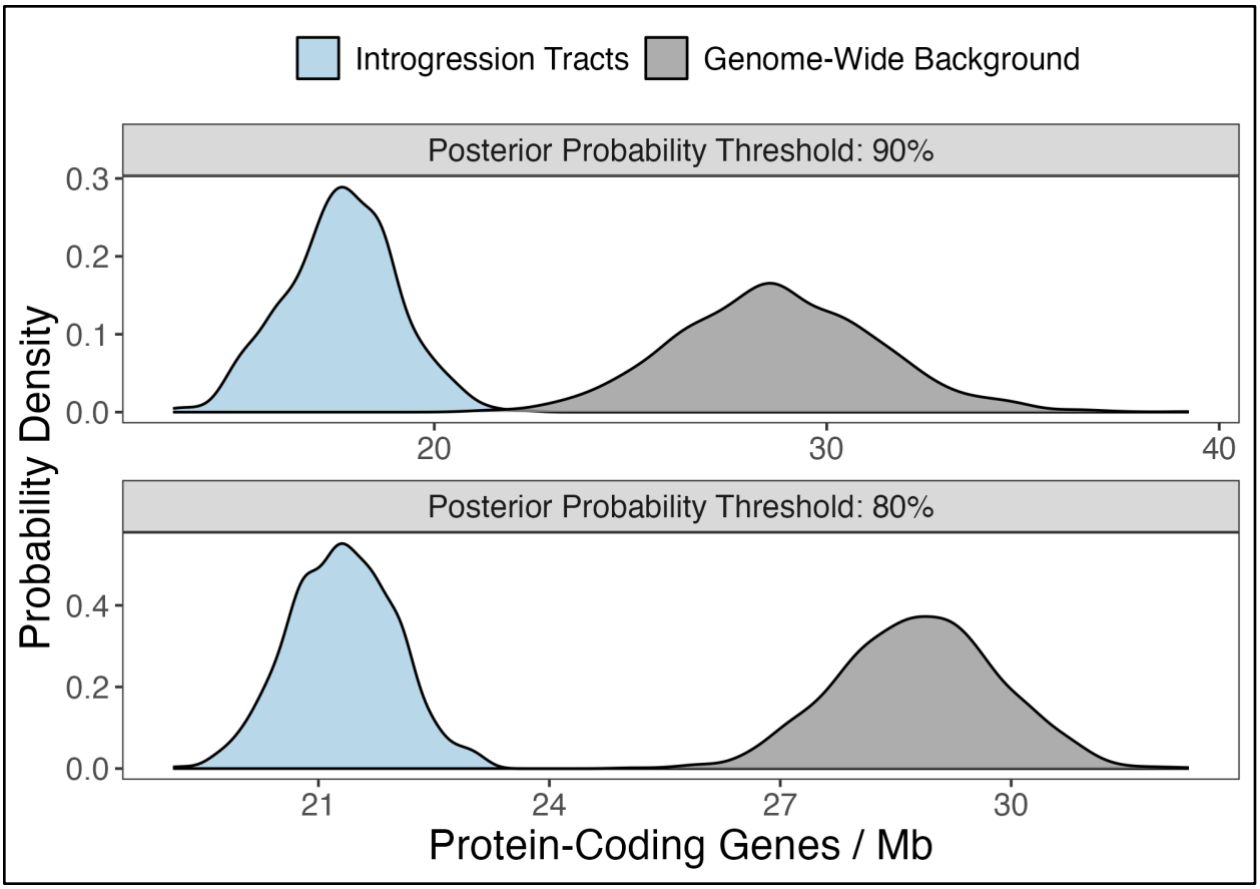

Figure S4. Probability density distribution of the number of protein-coding genes per megabase for introgression tracts greater than 10 kb in length and the genome-wide background.

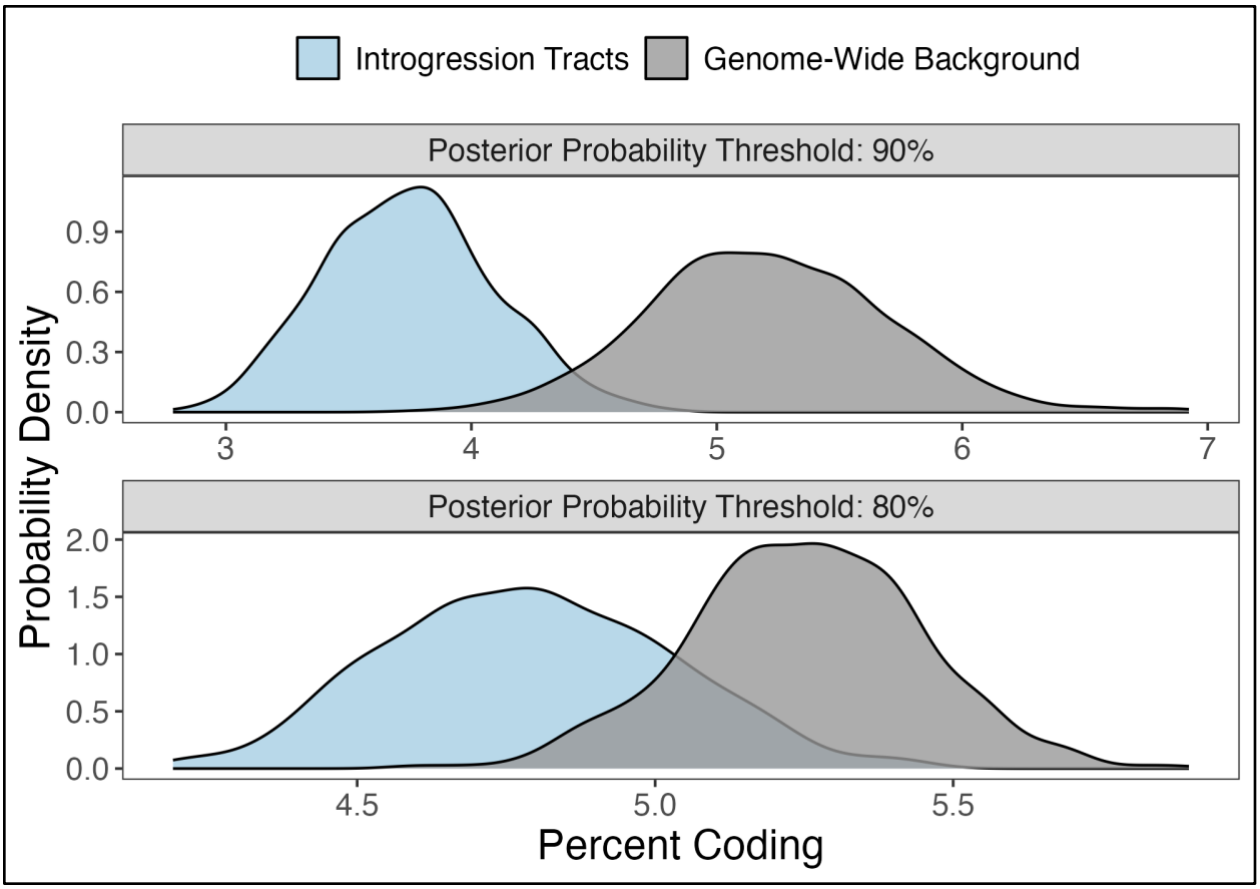

Figure S5. Probability density distribution of the percentage of coding bases for introgression tracts greater than 10 kb in length and the genome-wide background.

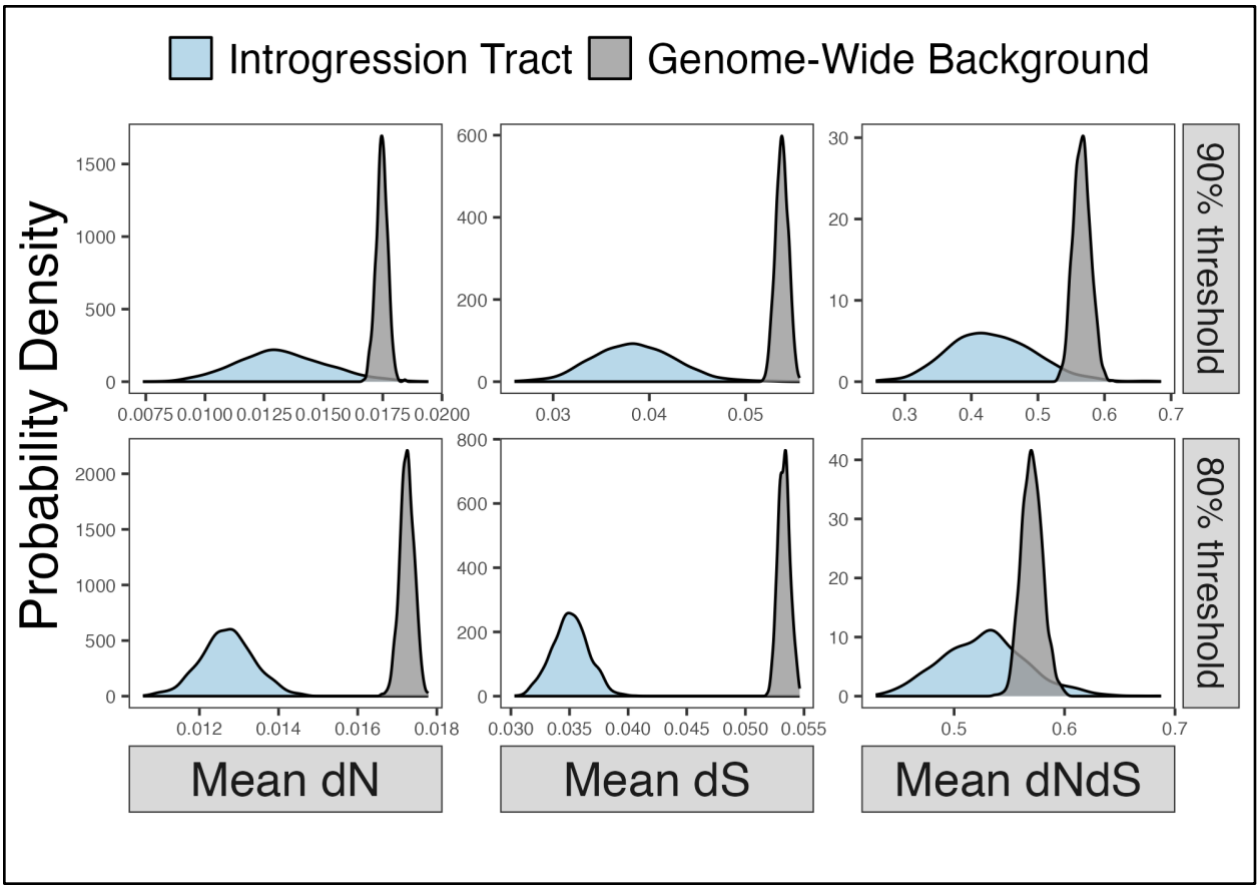

Figure S6. Probability density distribution for the mean *H. pulcherrimus* - *S. fragilis* d_N, d_S, and d_N/d_S for introgression tracts greater than 10 kb in length and the genome-wide background.